Atmos. Chem. Phys., 25, 1289–1305, 2025
https://doi.org/10.5194/acp-25-1289-2025

Atmospheric Chemistry and Physics
Open Access
EGU

Transport into the polar stratosphere from the Asian monsoon region

Xiaolu Yan[1], Paul Konopka[2], Felix Ploeger[2,3], and Aurélien Podglajen[4]

[1]State Key Laboratory of Severe Weather, Chinese Academy of Meteorological Sciences, Beijing, China
[2]Institute for Energy and Climate Research: Stratosphere (IEK-7), Forschungszentrum Jülich, Jülich, Germany
[3]Institute for Atmospheric and Environmental Research, University of Wuppertal, Wuppertal, Germany
[4]Laboratoire de Météorologie Dynamique (LMD/IPSL), École Polytechnique, Institut Polytechnique de Paris, Sorbonne Université, École Normale Supérieure, PSL Research University, CNRS, Paris, France

Correspondence: Xiaolu Yan (xiaoluyan@cma.gov.cn) and Paul Konopka (p.konopka@fz-juelich.de)

Received: 15 March 2024 – Discussion started: 22 March 2024
Revised: 11 November 2024 – Accepted: 27 November 2024 – Published: 29 January 2025

Abstract. The Southeast Asian boundary layer has witnessed alarming pollution levels in recent years, which even affects the trace gas composition in the Southern Hemisphere by inter-hemispheric transport. We use SF_6 observations and the Lagrangian chemistry transport model Chemical Lagrangian Model of the Stratosphere (CLaMS), driven by the ERA5 reanalysis data for the period 2010–2014, to assess the impact of the Asian monsoon (AM) region (15–45° N, 30–120° E) as a significant source of pollutants for the stratosphere, in particular in polar regions. We examine the contribution of transport from the AM region to the Northern Hemisphere polar region (NP) (60–90° N) and to the Southern Hemisphere polar region (SP) (60–90° S). Despite the smaller geographical size of the AM region when compared to the Southern Hemisphere subtropics (15–45° S) and the tropics (15° S–15° N), our findings reveal that the air mass fractions from the AM to the polar regions are approximately 1.5 times larger than the corresponding contributions from the Southern Hemisphere subtropics and only about 2 times smaller than those from the tropics. The transport of air masses from the AM boundary layer to the stratospheric polar vortex primarily occurs above an altitude of about 450 K and over timescales exceeding 2 years. In contrast, transport timescales to the polar regions situated below the vortex are shorter, typically less than about 2 years. Furthermore, the transport contribution from the AM region to the polar regions exhibits distinctive inter-annual variability, significantly influencing the distributions of pollutants. Our analysis of detrended SF_6 from an Atmospheric Chemistry Experiment Fourier transform spectrometer (ACE-FTS) over the polar regions reveals a strong correlation with the fraction of relatively young air (less than 2 years old) originating from the AM, Southern Hemisphere subtropics, and the tropics. Importantly, our reconstructed SF_6 data indicate that approximately 20 % of SF_6 in both the northern and southern polar stratosphere originates from the AM boundary layer. The largest fraction of SF_6 in the polar stratosphere still originates from the tropical boundary layer, contributing about 50 % of SF_6.

1 Introduction

Over the past few decades, rapid economic development in Southeast Asia has been associated with a notable increase in the emissions of various pollutants, including SO_2, NO_x, ozone precursors, particulate matters, and others (e.g. Granier et al., 2011; Kurokawa et al., 2013; Anenberg et al., 2019; Tessum et al., 2022). According to the Emissions Database for Global Atmospheric Research (EDGAR), Southeast Asia reports the largest emissions of the three major long-lived greenhouse gases (CO_2, CH_4, and N_2O) when compared to other continents (Janssens-Maenhout et al., 2019). Additionally, data from the TROPOspheric Monitoring Instrument (TROPOMI) and the Copernicus Atmo-

sphere Monitoring Service (CAMS) reveal elevated total CO column values and anthropogenic CO emission inventories over Asia (e.g. Y. Wang et al., 2022).

The elevated emissions of CO, PAN, ozone, HCFC-22, CH_2Cl_2, CH_3Cl, CH_3CN, CH_3OH, HNO_3, and HCl within the Asian boundary layer have potential impacts on the chemical composition of the atmosphere, thereby influencing atmospheric chemistry, radiative properties, climate, and human health (e.g. Berntsen et al., 1999; Park et al., 2009; Riese et al., 2012; Chirkov et al., 2016; Santee et al., 2017; Rolf et al., 2018; Bian et al., 2020; Adcock et al., 2021; H. Wang et al., 2022; Ma et al., 2024). Black carbon and greenhouse gases contribute to global warming, especially in the Arctic, by absorbing sunlight and reducing the reflectivity of snow and ice, leading to accelerated melting and altering climate patterns. Ozone precursors, tropospheric ozone, SO_2, and NO_x cause adverse health effects as well as contribute to the degradation of ecosystems. Exposure to particulate matter and other pollutants can lead to respiratory diseases, cardiovascular problems, and other health issues. The World Health Organization has linked air pollution to millions of premature deaths worldwide. These impacts extend beyond the local boundary layer, significantly affecting the upper troposphere and lower stratosphere (UTLS) (e.g. Dethof et al., 1999; Vernier et al., 2011; Vogel et al., 2016; Fadnavis et al., 2018). Particularly the Asian summer monsoon (ASM) circulation, which dominates the UTLS in the Northern Hemisphere (NH) during boreal summer, serves as an efficient pathway for transporting pollutants from the Asian boundary layer to the stratosphere over Asia and the tropics (e.g. Randel et al., 2010; Yu et al., 2017; Bian et al., 2020). Through this transport pathway, Southeast Asian emissions might affect the atmospheric composition inside the ASM anticyclone and in the tropical lower stratosphere. These changes may then propagate horizontally along isentropic surfaces and vertically through the Brewer–Dobson circulation (BDC), ultimately influencing the stratosphere, even at high latitudes (e.g. Park et al., 2013; Vogel et al., 2015; Pan et al., 2016; Ploeger et al., 2017).

Numerous observational studies have provided compelling evidence of the presence of high levels of tropospheric tracers within the ASM anticyclone, including water vapour, CO, and aerosols (e.g. Park et al., 2009; Vernier et al., 2011; Santee et al., 2017). Several previous studies have investigated the transport of ASM origin tracers to the global stratosphere (e.g. Wright et al., 2011; Bergman et al., 2012; Orbe et al., 2015), all of which underscore the dominant role played by the ASM in transporting tropospheric air into the stratosphere. Furthermore, some other studies aimed to quantify the specific contributions of tracers originating from the ASM anticyclone to the stratosphere. For instance, Garny and Randel (2016) calculated trajectories originating from the ASM anticyclone and found that 48 % of these trajectories reach the stratosphere within 60 d, with 24 % and 15 % of trajectories subsequently transported to the tropics and the lower stratosphere of the NH, respectively. Consequently, the ASM anticyclone contributes 14 % and 29 % of water vapour to the tropical pipe and to the NH extratropical lower stratosphere, respectively (Nützel et al., 2019).

Many previous studies have primarily focused on assessing the transport from the Asian monsoon (AM) region to the tropics and the NH (e.g. Tzella and Legras, 2011; Orbe et al., 2015; Yu et al., 2017). However, relatively little scientific attention has been devoted to understanding the contribution of the AM boundary layer to the polar stratosphere and its quantitative impact on pollutants, particularly in the southern polar stratosphere. Montzka et al. (2018) reported an unexpected global increase in the levels of ozone-depleting CFC-11, primarily attributed to a rise in emissions from eastern Asia after 2012. The depletion of the ozone layer caused by CFC-11 and also very short-lived substances (e.g. brominated substances) leads to increased UV exposure, which can cause skin cancer, cataracts, and immune system suppression in humans (e.g. Bais et al., 2018; World Meteorological Organization, 2022). Ozone depletion is particularly severe in polar regions due to cold temperatures and the presence of polar stratospheric clouds, which accelerate ozone destruction (e.g. Tritscher et al., 2021; World Meteorological Organization, 2022). Ploeger et al. (2017) released artificial tracers from the ASM anticyclone level and found a strong correlation between ASM origin air and HCN observations from the Atmospheric Chemistry Experiment Fourier transform spectrometer (ACE-FTS) satellite instrument. HCN is highly toxic to humans even at low concentrations. Yan et al. (2019) found that a greater quantity of ASM origin air is transported to the Southern Hemisphere (SH) compared to the NH after 9 months, when the simulated tracers are released below the tropopause. Hence, air pollutants from the AM region have the potential to affect the global environment and human health.

Motivated by these previous studies, our research particularly aims at examining the transport of air masses from the AM region into the stratosphere. This investigation is particularly crucial due to the sensitive climate effect associated with anthropogenic activity and the complex atmospheric chemical effect related to the ozone hole over polar regions (e.g. Clem et al., 2020; World Meteorological Organization, 2022). Our primary goal is to quantitatively assess the air mass fraction (AMF) originating from the AM region that reaches the polar stratosphere and its impact on pollutants. To achieve this goal, we utilize ERA5 reanalyses to drive the Chemical Lagrangian Model of the Stratosphere (CLaMS), enabling us to analyse AMFs and transit times from the source region into the polar stratosphere and to validate the simulations. Additionally, we reconstruct SF_6 data through a combination of surface boundary measurements and model simulations, facilitating the quantification of SF_6 transport contributions from the AM region to polar regions. Section 2 presents the data and methods used for our analyses. In Sect. 3, we explore the seasonality of transport

from the AM region and other source regions, along with a comprehensive diagnosis of the transport into the polar region. We investigate the influence of transport from the AM region on the SF_6 and assess the quantitative contributions in Sect. 4. Finally, we discuss our findings in Sect. 5, followed by a summary of the key results in Sect. 6.

2 Data and methods

In this study, we employ the CLaMS model to calculate age spectra and AMF to investigate transport processes originating from the surface of the AM region, defined as the area spanning 15–45° N and 30–120° E. CLaMS, a Lagrangian chemistry transport model (CTM), simulates trace gas transport driven by horizontal winds and total diabatic heating rates derived from reanalysis data (e.g. McKenna et al., 2002; Konopka et al., 2004; Pommrich et al., 2014). The destination regions are defined as the lower stratosphere of the northern polar region (polarLS-NH: 45–90° N) and the lower stratosphere of the southern polar region (polarLS-SH: 45–90° S). For comparison, we divide the Earth's surface into five distinct regions to compare transport contributions. These regions include the Northern Hemisphere extratropics (extNH: 45–90° N), Northern Hemisphere subtropics (subTR-NH: 15–45° N), tropics (15° S–15° N), Southern Hemisphere subtropics (subTR-SH: 15–45° S), and Southern Hemisphere extratropics (extSH: 45–90° S). The source domains and destination regions for this study are listed in Table 1.

We apply the Boundary Impulse (time-)Evolving Response (BIER) approach to calculate the age spectrum following the methodology outlined in Ploeger and Birner (2016). The BIER approach is an extension of the boundary impulse response (BIR) method (e.g. Haine et al., 2008; Li et al., 2012) such that the method evolves with time in a transient simulation. The approach in this work is similar to our previous study in Yan et al. (2021), albeit focusing on different source regions. We initiate multiple tracer pulses within the respective boundary source regions, denoted as Ω_i, with i representing the source domain (e.g. AM, NH extratropics, NH subtropics, tropics, SH subtropics, SH extratropics). The passive tracer, characterized by its mixing ratio χ_i at location r and time t, is related to the mixing ratio $\chi_0(t)$ originating from the boundary surface of various source regions. This relationship defines the AMF from the respective source regions and can be expressed as follows:

$$\chi_i(r,t) = \int_0^\infty \chi_0(\Omega_i, t-\tau)\, G(r,t|\Omega_i, t-\tau)\, \mathrm{d}\tau. \quad (1)$$

The age spectrum G is computed by releasing 240 pulses of inert trace gas species from six distinct source regions, with each region pulsing 40 different species. All the 40 species are artificial pulse tracers in the model for the age spectrum calculation. These pulse tracers approximate a δ distribution lower boundary condition $\chi_0^j(\Omega_i, t) = \delta(t - t_j)$, where j ranges from 1 to 40, defining the tracer pulses at specific source times t_j. The pulse tracer mixing ratios are initially set to 1 within the boundary layer of the source region for a duration of 30 d. Outside of the initialization region, these mixing ratios in the boundary are set to zero in each time step. The 40 species are passive tracers without chemistry involved in the simulations, which represent the air released at different times within 10 years. To elaborate further, the first 24 different species ($j = 1, \ldots, 24$), characterized by transit times of less than 2 years, are pulsed every month. Subsequently, the remaining 16 different species ($j = 25, \ldots, 40$) are pulsed every 6th month (the 25th species is pulsed in the 30th month, the 26th species in the 36th month, and so on). Consequently, all species have been pulsed after 10 years of model simulation. A total of 10 years after release, the pulse tracer mixing ratio is set to zero again throughout the entire atmosphere and subsequently pulsed again. As a result, the model simulations provide a monthly-resolution age spectrum for transit times shorter than 2 years and a semi-annual-resolution age spectrum for longer transit times. For additional details regarding the model set-up and the calculation of age spectra from multiple pulse tracers, please refer to Ploeger and Birner (2016), Ploeger et al. (2019), Podglajen and Ploeger (2019), and Yan et al. (2021).

To quantify the contributions of surface origin air from the six regions to stratospheric pollutants, we carry out the reconstruction of SF_6 data using age spectrum simulations in conjunction with surface composition observations from the National Oceanic and Atmospheric Administration (NOAA, Dutton et al., 2024). SF_6, characterized by an atmospheric lifetime of approximately 3200 years, remains virtually unaltered in the atmosphere for many centuries following its emission. Consequently, SF_6 serves as a valuable tracer for evaluating transport in models and calculating mean ages (e.g. Denning et al., 1999; Waugh et al., 2013). The reconstructed SF_6, characterized by its mixing ratio at location r and time t, is related to the SF_6 concentration emitted from the boundary layer of various source regions. This defines the reconstructed SF_6 concentration transported from the respective source regions and can be calculated following Eq. (1). However, in the case of SF_6, $\chi_0(t)$ is the SF_6 mixing ratio at the boundary layer in the respective surface patch.

We employ observations of SF_6 obtained from the Atmospheric Chemistry Experiment Fourier transform spectrometer (ACE-FTS) satellite instrument (e.g. Bernath et al., 2005) to validate the reconstructed SF_6 data. In this study, our simulation encompasses the period from 2000 to 2014, driven by meteorological data from ERA5 reanalyses. Due to the 10-year spin-up time required for the air mass and age spectra, we focus on analysing the model data and ACE-FTS observations specifically from 2010 to 2014 in the following section. It is worth noting that the truncation of calculated age spectra to 10 years could cause a high bias in reconstructed SF_6 mixing ratios in the stratosphere. This time frame aligns with

Table 1. List of all source regions used in the model simulations and destination regions investigated by this study.

Source	Latitude	Longitude	Destination	Latitude	Longitude
AM	15–45° N	30–120° E	polarLS-NH	60–90° N	0–360°
extNH	45–90° N	0–360°	polarLS-SH	60–90° S	0–360°
subTR-NH	15–45° N	0–360°			
tropics	15° S–15° N	0–360°			
subTR-SH	15–45° S	0–360°			
extSH	45–90° S	0–360°			

the period analysed in Yan et al. (2019), allowing for a direct comparison between different experimental set-ups, including boundary layer and tropopause source domains, as well as 10 years and 1 year of simulated duration.

3 Air mass fractions from the Asian monsoon boundary layer

In this section, we quantify the air mass fractions transported from the boundary layer of the source domains. Our investigation explores the transport of air originating from all the source regions to the global stratosphere, utilizing artificial tracers released at the surface layer. The transport contributions to the global stratosphere from both the NH extratropics and SH extratropics are small, each accounting for less than 0.5 %. Consequently, we will not present detailed discussions regarding the results from these two source regions in this study.

3.1 Transport contributions from boundary layer source regions to the global stratosphere

To assess the global contributions originating from the AM region, we calculate zonally averaged seasonal mean AMFs from the AM boundary layer (Fig. 1, left panels). The transport characteristics from the subTR-NH exhibit significant similarities to those from the AM region; therefore, we do not present results for the subTR-NH in this study. In contrast, we illustrate the AMFs from the same latitude band as for the AM region but in the Southern Hemisphere (subTR-SH) (Fig. 1, middle) to explore hemispheric differences. Additionally, for reference, we include the AMFs from the tropics (Fig. 1, right). The contributions from the source regions to the stratosphere below 450 K are strongly affected by the distance between source regions and destination regions. Despite the fact that the AM region is approximately 4 times smaller than the subTR-SH, the contributions of air masses from the AM region to the global stratosphere above 450 K, including the southern hemispheric stratosphere, are approximately 1.5 times larger than the corresponding contributions from the subTR-SH. However, it is important to note that the AMFs originating from the AM region to the global stratosphere above 450 K are approximately 2–3 times smaller than those originating from the tropics.

The transport of newly released AM air into the NH stratosphere is initiated during boreal summer such that its impact on the NH stratosphere is at its maximum during boreal autumn. The AM origin tracers are also transported to the tropical pipe and the SH in the following seasons. Transport patterns from the subTR-SH to the stratosphere exhibit a lot of similarities to those originating from the AM, albeit with a 6-month time shift. It is noteworthy that more than 50 % of the stratospheric air is transported from the tropics, representing the largest contribution to the global stratosphere among all the source regions. The AM air tends to accumulate in the polar middle stratosphere, particularly above approximately 450 K. In the tropics, the AM origin air fraction is lower due to wintertime air ascending. However, a lot of AM origin air is transported to the high-latitude region during summer driven by the ASM circulation, while the AM origin air is more suppressed and isolated inside the source region during winter. Hence there is evidently a surplus of summertime air compared to wintertime air making its way into the high-latitude region.

We use zonal wind to examine the dynamic factors influencing transport from the source regions. During the boreal summer (June–August: JJA), the jet streams in the NH and SH exhibit differing characteristics, with the NH jet being relatively weak and the SH jet being notably strong. During the subsequent seasons of September–November (SON) and December–February (DJF), the tropical easterlies and SH jets tend to weaken, while the NH jet intensifies. The strength of the polar vortex plays a pivotal role in governing the transport of newly released tracers. A weak polar vortex facilitates the transport of tracers into the polar stratosphere, while a strong polar vortex effectively isolates stratospheric air within the polar regions. Notably, during DJF, the polar vortices in the NH and SH reach their strongest and weakest phases, respectively. The strong Pacific westerly ducts during boreal autumn and winter enable large cross-hemispheric transport (see Yan et al., 2021).

To explore the seasonal variation in transport from the boundary layer, we remove the annual mean contributions from each source region. These seasonal anomalies of the climatological zonal mean AMFs are depicted in Fig. 2, showcasing data from the AM region (left), subTR-SH (middle), and the tropics (right). While the absolute contributions from

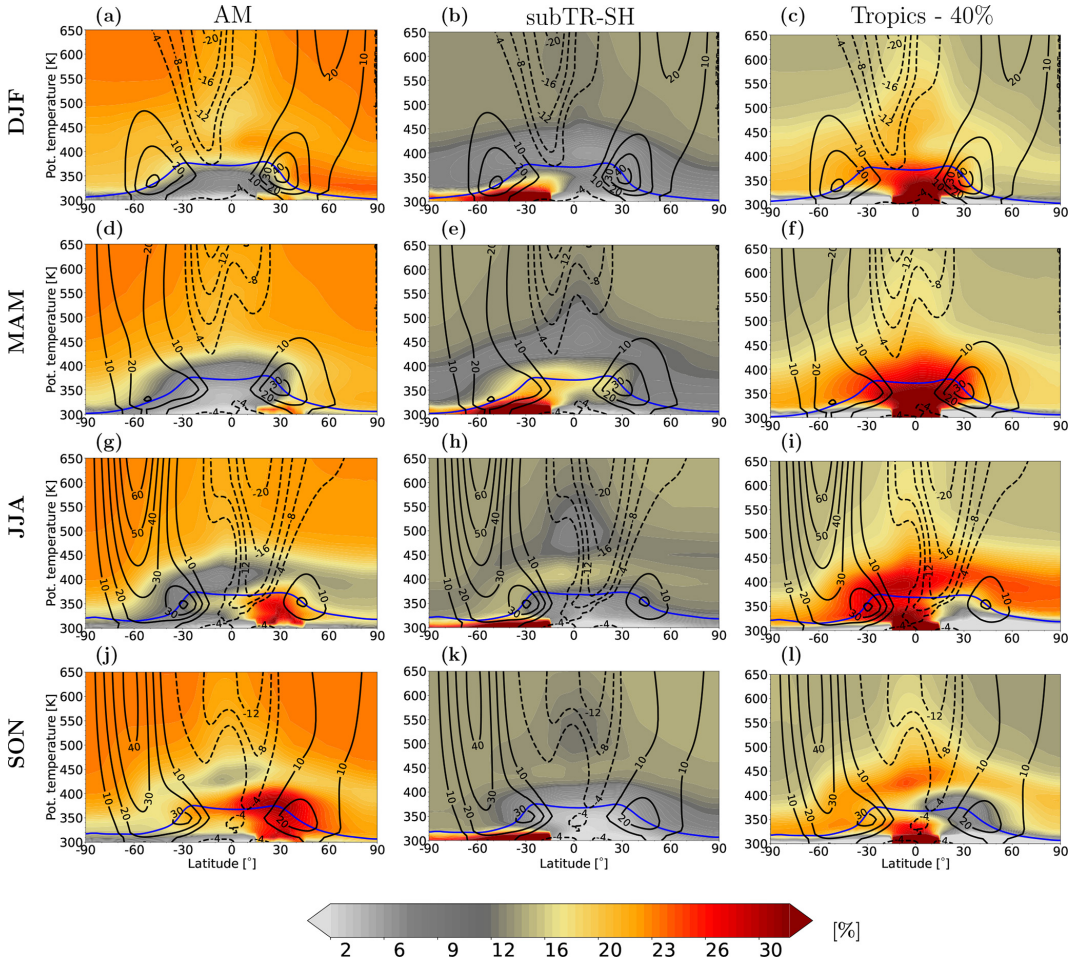

Figure 1. Climatological (2010–2013) zonal mean wind (black contours) and air mass fractions (colour shading) originating from the AM (15–45° N, 30–120° E, **a, d, g, j**), SH subtropics (15–45° S, **b, e, h, k**), and the tropics (15° N–15° S, **c, f, i, l**) for different seasons (rows). The blue line shows the WMO tropopause. Note a 40 % mass fraction has been subtracted from the tropical mass fraction for plotting.

the AM, subTR-SH, and the tropics differ significantly, the amplitude of the AMF seasonal cycle in the global UTLS, originating from these three source regions, demonstrates comparable values. Evidently, newly released AM air is primarily limited to the troposphere during boreal summer and is transported deeply to the stratosphere during boreal autumn and winter. During boreal summer, air of AM origin is more confined to the NH. However, as boreal autumn sets in, these air masses undergo inter-hemispheric transport, particularly below the tropical tropopause, which may be associated with the Hadley circulation. In the following seasons, AM origin air is transported into the SH extratropics through the UTLS, driven by the BDC. Transport patterns from the subTR-SH to the stratosphere exhibit considerable similarities to those from the AM region. It is noteworthy that subTR-SH air mass anomalies portray entirely negative values in the lower stratosphere above the SH extratropics during the months of March–May (MAM; Fig. 2e). In contrast, transport patterns from the tropics demonstrate nearly the opposite sign compared to those from the AM region. Tropical and AM origin air tend to compensate for each other within the atmosphere. Combined, the total tracer contributions from these two source regions amount to approximately 80 % of the AMFs in the global atmosphere.

In Fig. 2, the total diabatic heating rate (black contours) reveals pronounced downward motion in the northern polar stratosphere during SON and DJF. This downward motion effectively isolates a significant portion of the stratospheric air originating from the AM region within the Arctic polar vortex above 450 K (Fig. 2a and j). During JJA, the Arctic stratosphere experiences its weakest westerly jet (Fig. 1i), allowing for the substantial transport of newly released tropical air into the Arctic stratosphere between the tropopause and 450 K (Fig. 2i). This suggests that transport contributions from the tropics to the Arctic lower stratosphere are particularly influenced by quasi-horizontal isentropic transport.

Notably, the seasonality of the total diabatic heating rate over the Antarctic region exhibits a nearly 6-month shift

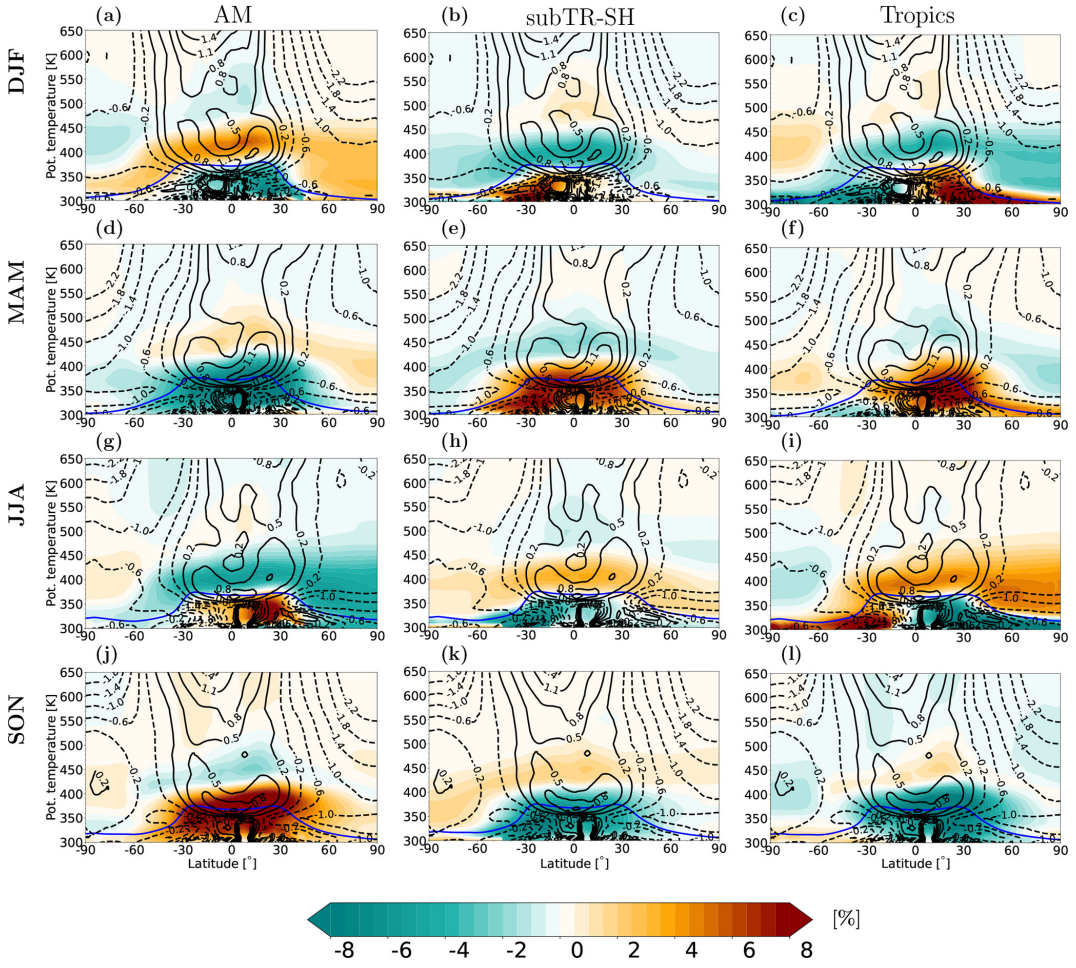

Figure 2. Climatological (2010–2013) air mass fraction (AMF) anomaly displayed as the departure from the annual average (colour shading), overlaid with ERA5 zonal mean total diabatic heating rates (black contours). The thick blue line represents the WMO tropopause.

compared to that over the Arctic. In the Antarctic region, strong downwelling occurs during MAM and JJA, leading to the accumulation of significant AM origin tracers (Fig. 2g). The largest amount of tropical tracers is transported into the Antarctic during DJF due to the weakened jet barrier and downwelling over the SH extratropics (Figs. 1c and 2c). In summary, more AM tracers are transported to the polar stratosphere during local autumn and winter, while a greater quantity of tropical tracers is transported to the polar stratosphere during local summer.

3.2 Transport timescales to the polar stratosphere as inferred from the age of air spectrum

In this subsection, we investigate the transport from the source regions into the polar regions specifically. Therefore, we analyse age spectra along the latitudes of 60° N and 60° S and present the results in Figs. 3 and 4, respectively. Examining the age spectra of air originating from the AM, subTR-SH, and the tropics along 60° N latitude (Fig. 3) reveals a clear seasonality in transport into the Arctic region, particularly for air from the AM and subTR-SH source regions. Below about 450 K, transport from the boundary layer of the AM, subTR-SH, and the tropics to the Arctic region occurs mainly on timescales smaller than about 2 years. Above 450 K, on the other hand, transport timescales to the northern polar vortex are generally longer than 2 years. The separation in the age spectra below/above 450 K and transit times shorter/longer than 2 years might indicate the separation between shallow and deep branches of BDC. Notably, the air from the three source regions exhibits its youngest mean age of air (AoA) in SON over the Arctic below 450 K.

The age spectrum of air originating from the AM region exhibits large values when the tracers are released during boreal summer (JJA); hence the probability of transport to the polar lower stratosphere is at a maximum for air masses released at the surface during summer. Conversely, these values are nearly zero when the AM origin tracers are released during boreal winter (DJF), strongly suggesting that pollutants from the AM region are primarily transported to the Arctic

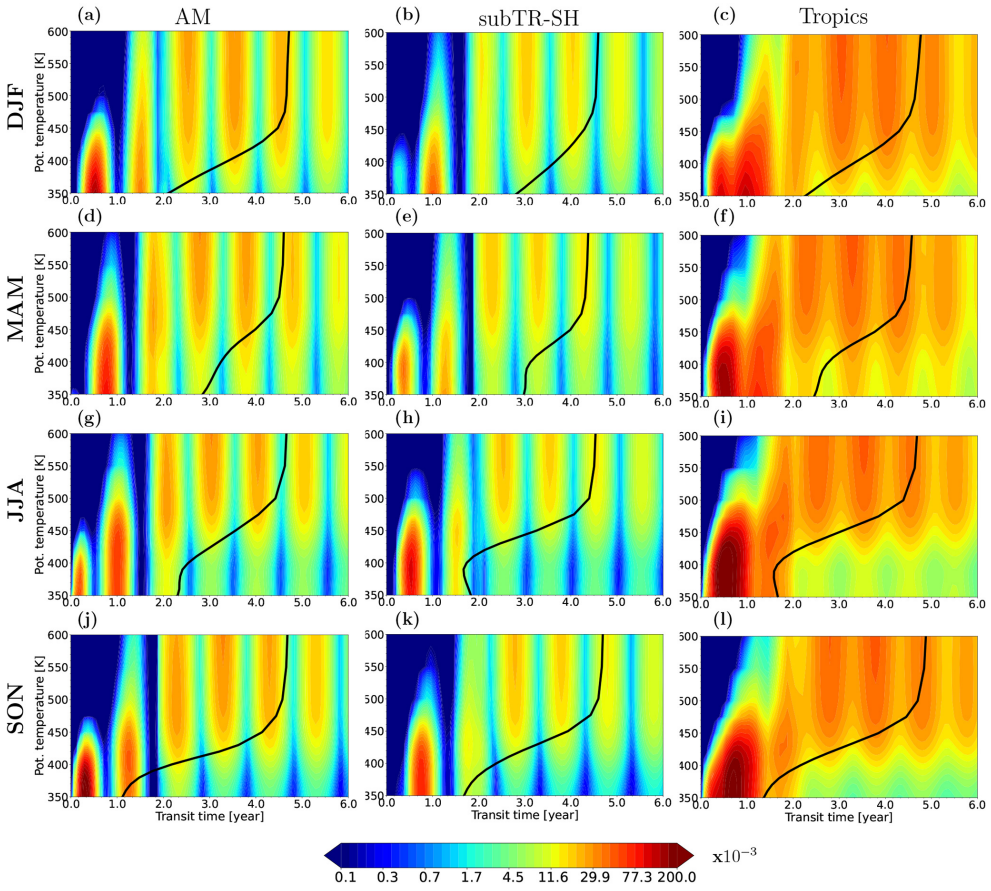

Figure 3. Age spectra as (partial) transit time probability density functions (PDFs), calculated for air originating from three source regions: AM, SH subtropics, and the tropics. Age spectra are shown along 60° N for all seasons. The black line shows the mean AoA as derived from the age spectrum.

stratosphere during boreal summer and autumn. In contrast, the primary contributions from the subTR-SH and tropics to the Arctic occur during austral summer (DJF). The age spectrum of AM origin air shows the larger partial contribution to the Arctic compared to that from the subTR-SH; both of them are evidently smaller than that originating from the tropics. Additionally, the transport patterns of subTR-SH and tropical origin air exhibit a lot of similarities, with a 6-month shift compared to the AM origin air. Transit times from the AM to the Arctic are longer (shorter) than those from the subTR-SH and tropics during JJA (DJF) below 450 K. The efficient transport from the subTR-SH to the Arctic might be driven first by the upper branch of the Hadley cell from the source region to the tropics and then by the quasi-horizontal isentropic transport from the tropics to the Arctic. For the AM air, it is more confined inside the Asian summer monsoon anticyclone in JJA and slowly ascending due to weak diabatic heating rates, and it might take a longer time to escape the anticyclone above Asia.

The age spectra along 60° S, as presented in Fig. 4, exhibit numerous similarities to those observed along 60° N. Specifically, the probability density functions (PDFs) display substantial values below (above) the lower stratosphere, corresponding to transit times shorter (longer) than 2 years. The age spectra from both 60° N and 60° S show the different impacts of deep and shallow branches of BDC on the transport of air masses into the polar regions. The age spectra along 60° S also show distinct seasonal-cycle features. The PDFs along this latitude reveal peaks and nadirs at transit times similar to those along 60° N. This recurring pattern underscores the fact that pollutants from the source regions released during local summer (JJA for AM and DJF for SH subtropics) have the highest chance to be transported to the Antarctic stratosphere, while pollutants released during the winter face greater difficulty in distant transport.

Despite the similarities, it is noteworthy that the values of the PDFs along 60° S latitude are notably smaller when compared to those along 60° N. This fact holds true even for the subTR-SH origin air despite the shorter distance between subTR-SH and the Antarctic region compared to the distance between subTR-SH and the Arctic. The variation in the vertical range of source tracers transported to the Antarc-

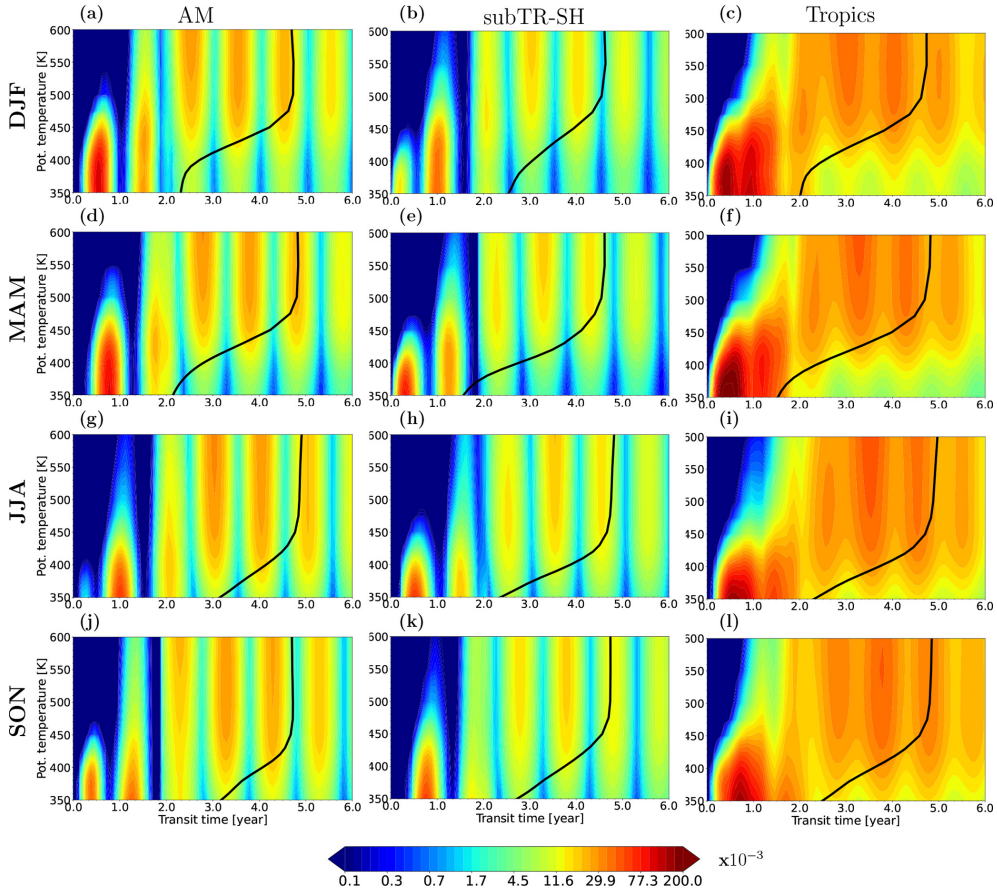

Figure 4. Same as Fig. 3 but for age spectra along 60° S.

tic stratosphere is likely related to the strength of the polar vortex. During austral winter (JJA), the source tracers experience a downward transport to lower levels over the Antarctic region compared to austral summer (DJF). Additionally, both the vertical range and vertical profile of the mean AoA originating from the three source regions along 60° S latitude exhibit a shift of approximately 6 months when compared to those observed along 60° N. Consequently, air from these three source regions over the Antarctic region exhibits its youngest mean AoA in MAM below 450 K.

3.3 Transport timescales to the polar lower stratosphere driven by the shallow branch of Brewer–Dobson circulation

The notable difference in age spectrum behaviour at different altitudes for transit times shorter and longer than 2 years has motivated our investigation into the contributions of source tracers transported to the polar regions with transit times of less than 2 years, potentially driven by the shallow branch of the BDC. In this way, our focus is directed more towards the short-lived boundary emissions transported into the polar regions, influenced more by fast isentropic transport and less by the upper branch of the BDC. In Fig. 5, we present AMFs and their anomalies with AoA lengths of less than 2 years which are transported to the northern polar region (60–90° N) and the southern polar region (60–90° S). Young air, characterized by an AoA of less than 2 years, originating from all three source domains is primarily transported to the polar regions below the polar vortex, and this transport decreases with increasing altitude (Fig. 5a–f). Interestingly, despite the smaller size of the AM region and the closer distance between the subTR-SH and the Antarctic region, the air mass contributions from the AM to the polar regions are even larger than those from the subTR-SH. However, both AM and subTR-SH contributions remain much smaller than those from the tropics. Furthermore, the tracers from all three source regions exhibit a greater transport into the northern polar region when compared to their transport into the southern polar region. Maximum and minimum AMFs from the three source regions over 60–90° N exhibit a 6-month shift when compared to those over 60–90° S. Specifically, air originating from the AM and subTR-SH regions displays peaks in the northern and southern polar regions during local autumn, while air from the tropics reaches its peak in the polar region during local summer.

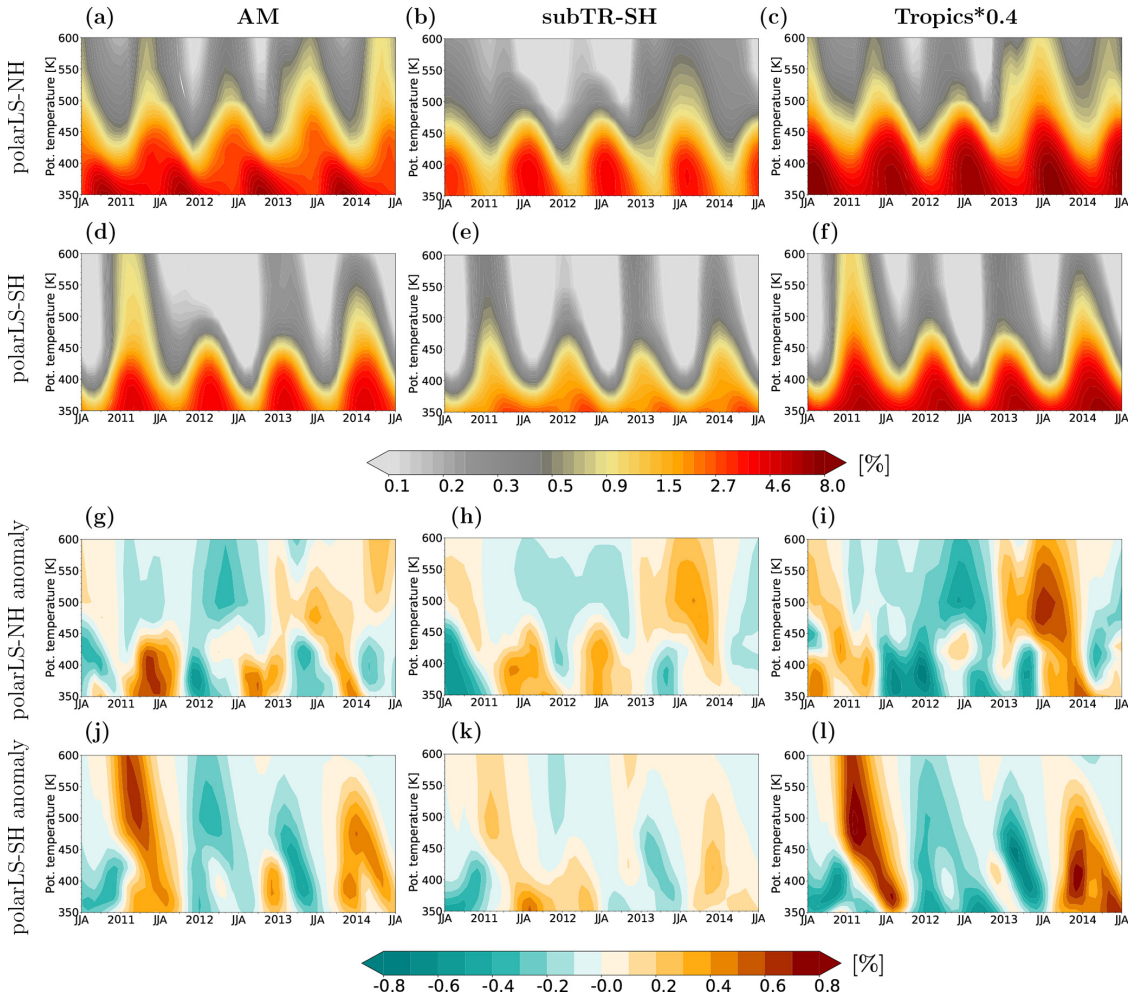

Figure 5. Potential temperature–time cross sections of young (< 2 years) air mass fractions **(a–f)** and anomalies **(g–l)** relative to the monthly mean value (2011–2014) originating from AM **(a, d, g, j)**, SH subtropics **(b, e, h, k)**, and the tropics **(c, f, i, l)** over 60–90° N and 60–90° S.

We perform deseasonalization on the AMFs transported from the source regions to the polar regions and present the results in Fig. 5g–l. Notably, there exists distinct inter-annual variability in the AMFs over the polar regions, and the magnitude of this variability is comparable between the northern and southern polar regions. These inter-annual variability patterns vary significantly across different vertical levels. The tracers transported to the polar regions display less variability above 450 K than below. The inter-annual variability in AMFs over the southern polar region exhibits a 6-month shift compared to that of the northern polar region. More frequent changes in the inter-annual variability below 450 K over the polar regions compared to the higher levels are likely driven by both downward propagation from higher altitudes and the shallow branch of the BDC. Despite the similarities, the inter-annual variability over the southern polar region (Fig. 5j–l) is more consistent throughout different levels compared to that over the northern polar region (Fig. 5g–i). In general, the westerly jets in the Southern Hemisphere are stronger than those in the Northern Hemisphere (see Fig. 1). Hence, the air in the southern polar stratosphere is strongly isolated and more affected by the downwelling of the deep branch of the BDC, while the air in the northern polar stratosphere is relatively less confined and more strongly affected by the deep branch of BDC, shallow branch of BDC, and quasi-horizontal isentropic transport.

4 Quantification of Asian monsoon impact on the polar stratospheric composition

Up to this point, we have calculated the contributions from the AM boundary surface layer and the other two source regions to the global stratosphere. Our investigation of the transport into the polar regions has revealed that long-term transport contributions from the AM to the polar regions fall within the range of 5 % to 20 %, depending on the altitude. It is worth noting that the AMFs originating from the AM boundary surface layer over the polar region below 450 K

are predominantly composed of air with transit times of less than 2 years. In this section, our objective is first to validate and then to quantify the impact of emissions from the AM boundary as well as other source regions on pollutant concentrations over the polar regions. We achieve this using SF_6 observations obtained from the ACE-FTS satellite instrument and reconstructed SF_6 data by using Eq. (1).

4.1 Evaluation of reconstructed SF_6 data

We utilize the AMFs originating from different source regions and zonally averaged SF_6 data from NOAA surface observations to reconstruct zonal mean SF_6 data in the whole atmosphere. Here, the original NOAA SF_6 surface observation data are used to estimate the mean transit time from station to station. Measurements of SF_6 are offset for each latitude by the corresponding transit time to get high-resolution latitudinal data. The reconstructed SF_6 data are calculated by averaging SF_6 surface observations from each source region, integrated with the corresponding AMFs originating from that same source region. To assess the accuracy of the reconstructed SF_6 data, our first step involves a comparison between the reconstructed data and SF_6 observations obtained from ACE-FTS. In Fig. 6a–d, we present the seasonal mean SF_6 concentrations from ACE-FTS (left) and the reconstructed data (right) for both the north polar region (a–b) and the south polar region (c–d). The comparison results reveal a strong agreement between the vertical distribution of the reconstructed SF_6 data and the ACE-FTS observations over the polar regions. The reconstructed SF_6 data are slightly smaller in the troposphere and larger in the stratosphere compared to ACE-FTS SF_6 data. This is likely due to underrepresented CLaMS vertical transport in the troposphere (Konopka et al., 2022), truncation of calculated age spectra to 10 years, and missing mesospheric SF_6 loss in the reconstruction. Nevertheless, both datasets exhibit rapid growth rates and distinct seasonality. Specifically, SF_6 concentrations over the northern polar region peak in SON, while those over the southern polar region peak in MAM. Furthermore, the abundance of SF_6 over the northern polar region is larger than that over the southern polar region.

To assess the reliability of the reconstructed SF_6 data, we implement a process of detrending and deseasonalizing SF_6 distributions over the polar regions. Figure 6e–h present the detrended and deseasonalized SF_6 data from both ACE-FTS and the reconstruction for both the north polar region and the south polar region. Upon examining the inter-annual variability over the polar regions without trends, the comparison shows clear similarities between the reconstructed SF_6 and ACE-FTS SF_6, and both of them also show similar features to the inter-annual variability in the three source-origin AMFs over the polar regions (refer to Fig. 5g–i). Notably, the detrended and deseasonalized SF_6 data for the northern polar region exhibit a clear positive anomaly during JJA in 2010 and 2013, particularly above 450 K. This positive anomaly subsequently propagates downward and leads to a positive anomaly in DJF of 2010 and 2013 below 450 K. Similar positive anomalies below about 450 K also occur in the JJA of 2011 and 2012, like the patterns observed for AM and subTR-SH origin air (see Fig. 5g and h).

In the Southern Hemisphere, both the reconstructed SF_6 and ACE-FTS SF_6 observations reveal inter-annual variability characterized by positive anomalies in 2011 and 2013. However, the positive anomaly observed in the reconstructed SF_6 data for 2012 does not align with the inter-annual variability in ACE-FTS SF_6 observations between 400 and 550 K. This discrepancy warrants further investigation. Overall, the inter-annual variability in the reconstructed SF_6 data without trends closely matches that observed in ACE-FTS SF_6 data over the polar regions. The reconstructed SF_6 data successfully capture most of the key features observed in ACE-FTS SF_6 data over the polar regions.

4.2 Contributions of SF_6 transport from source regions

The reconstructed SF_6 data have been validated with ACE-FTS SF_6 observations above. We now turn our attention to analysing the contributions of transport from each source region to the polar regions using the reconstructed SF_6 data. Figure 7 provides a comprehensive view, showcasing the reconstructed SF_6 concentrations alongside the relative contributions from AM, subTR-NH, subTR-SH, and TR for both the northern polar region (left) and the southern polar region (right). In the northern polar region, the SF_6 levels originating from the source regions exhibit an increasing trend from 2010 to 2014, with the exception of transport from TR in 2010. These concentrations display distinct seasonality within the lower stratosphere of the polar region. The transport contributions from AM and subTR-NH peak during DJF, while those from subTR-SH and TR reach their crest values in JJA. This might be related to the transit time in summer from source regions to the polar lower stratosphere, and pollutants released during the summer are more extensively transported to the polar regions compared to the winter emissions of pollutants from source regions as we discussed above in Sect. 3.2. Interestingly, despite increasing global boundary layer emissions from 2010 to 2014, the SF_6 concentrations transported from AM, subTR-NH, and subTR-SH to the polar region do not consistently exhibit an upward trend. This suggests that factors beyond emissions might exert a substantial influence on pollutant abundance in the southern polar region, such as the dynamics of the polar vortex and the BDC.

We normalize the SF_6 emissions from each source region by the total SF_6 from the global surface layer, which allows us to determine the relative contributions of SF_6 transport from each source region to the polar regions. Notably, the relative contributions of SF_6 from AM, subTR-NH, and subTR-SH to the polar regions above 450 K are greater than those to the regions below 450 K, while the tropics contribute more

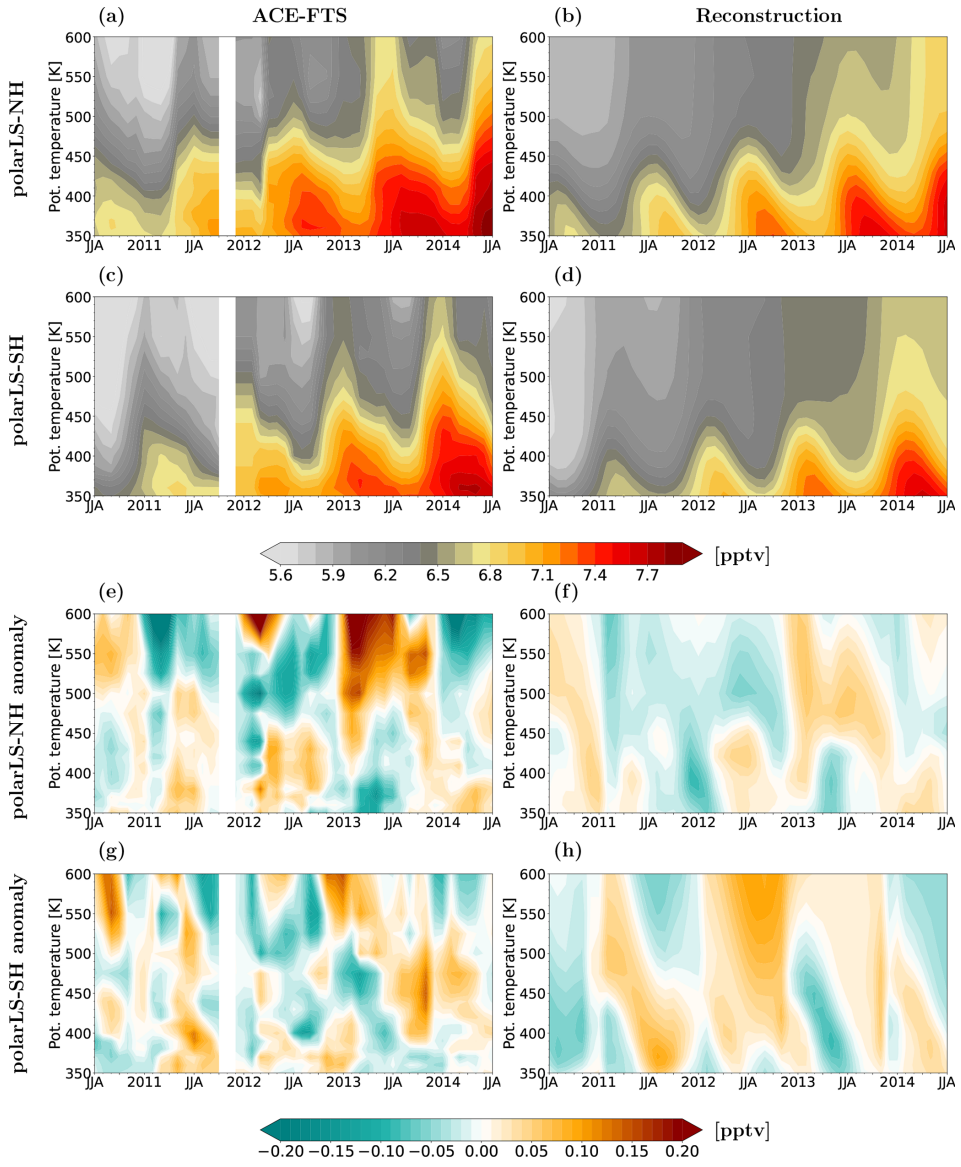

Figure 6. Potential temperature–time of seasonal mean SF_6 **(a–d)** of ACE-FTS **(a, c, e, g)** and reconstruction **(b, d, f, h)** over the north polar region (60–90° N) and the south polar region (60–90° S) and their detrended and deseasonalized distribution **(e–h)**.

to altitudes below 450 K in the polar regions. Specifically, AM contributes over 20 % of the SF_6 present in the polar stratosphere above 450 K, and remarkably, more than 70 % of the subTR-NH SF_6 in the polar region originates from AM transport. It is worth noting that the reconstructed SF_6 from the AM region is based on the zonally averaged SF_6 data from NOAA surface observations at the same latitude bands, which might even underestimate the contributions of SF_6 from the AM region. Moreover, the contributions of SF_6 from AM to the southern polar region slightly surpass those to the northern polar region, underscoring the significance of inter-hemispheric transport dynamics. Again, the SF_6 contributions from AM outstrip those from subTR-SH despite the smaller source domain of the AM region and the longer distance between AM and the southern polar region. Another interesting fact is that the positive SF_6 anomaly in the reconstruction over the southern polar region in 2012 (Fig. 6h) is related to particularly strong transport from the AM region (Fig. 7b), which warrants further investigation. The tropics still serve as the largest SF_6 source for the polar regions, accounting for over 50 % of SF_6 concentrations in the polar regions. Considering the size of their respective source domains, the transport of SF_6 from the AM boundary layer to the polar region proves to be more efficient compared to that from the tropical boundary layer.

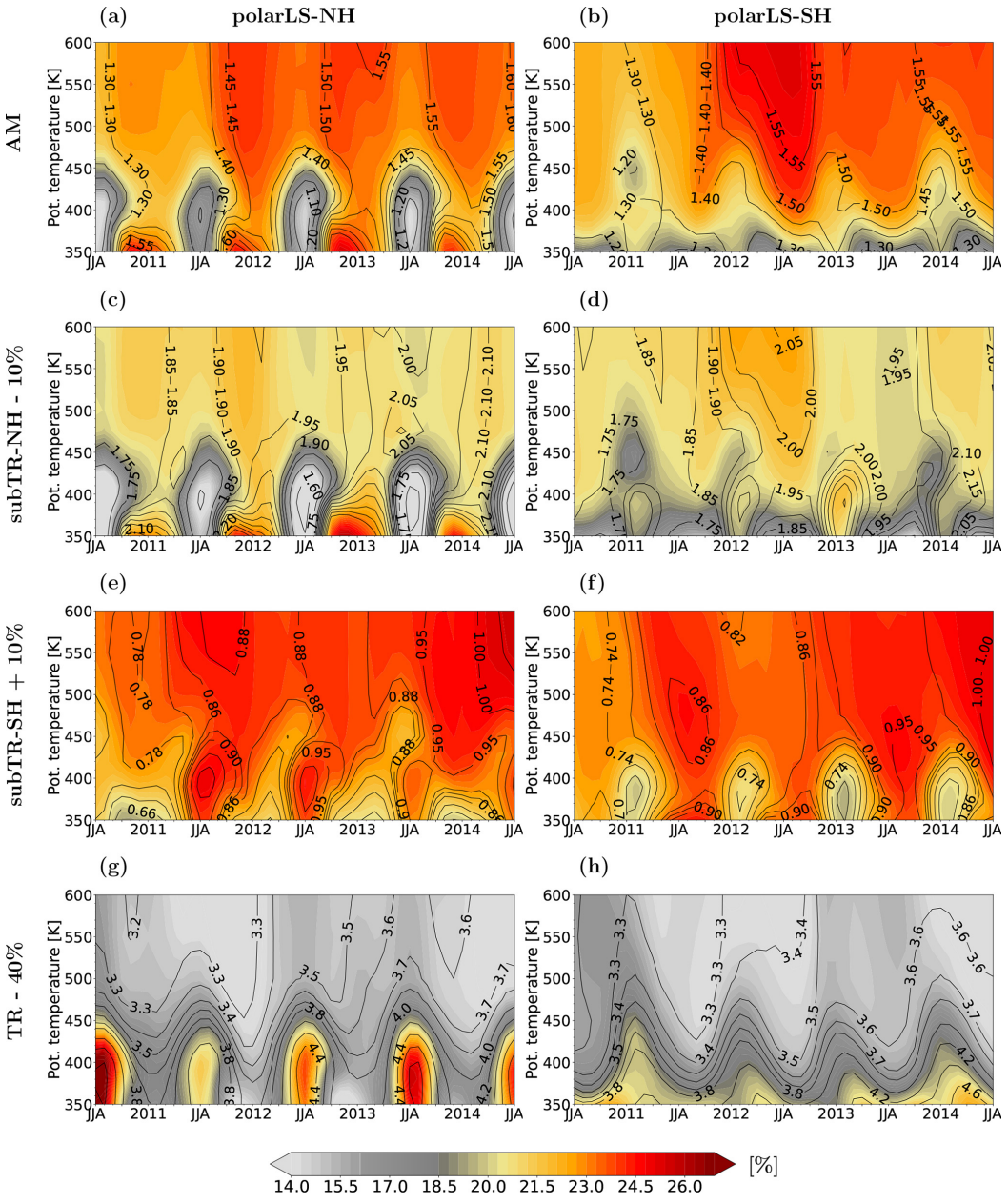

Figure 7. Potential temperature–time sections of reconstructed SF_6 (black contours) and relative contributions (colour shading) from AM **(a, b)**, NH subtropics **(c, d)**, SH subtropics **(e, f)**, and the tropics **(g, h)** over the north polar region (60–90° N, **a, c, e, g**) and the south polar region (60–90° S, **b, d, f, h**). Note that the relative contributions have been scaled for plotting.

5 Discussion

The transport of pollutants from Southeast Asia into the global stratosphere has attracted significant attention due to the rapid economic growth in this region and the unique pathway of transport through the ASM anticyclone. The quantification of this transport can be influenced by various methods, models, and reanalysis datasets. Previous studies by Garny and Randel (2016) and Yu et al. (2017) investigated the transport from the upper troposphere over the AM region, employing trajectory analyses and aerosol simulations, respectively. Ploeger et al. (2017) conducted an assessment of pollution transport from the ASM into the lower stratosphere using artificial tracers of air mass origin from the ASM anticyclone. Although the simulation periods and source domain sizes slightly differed across these studies, they collectively revealed that approximately 15 % of air parcels originating from the AM region are directed toward the extratropics of the NH, with less than 5 % reaching the extratropics of the SH. Furthermore, prior investigations based on 1-year

simulations also indicated that air of AM origin experiences peak transport to the northern polar lower stratosphere during September to November (e.g. Ploeger et al., 2017; Yu et al., 2017) and to the southern polar lower stratosphere from December to February (e.g. Yan et al., 2019). These findings align closely with the results obtained in the present study, which is based on a 10-year simulation.

One notable difference between our study and prior research lies in the inter-hemispheric contrast in transport contributions from the AM region to the polar stratosphere above 450 K. Our analysis reveals that the contributions from the AM to the southern polar stratosphere and the northern polar stratosphere are roughly equivalent, both exceeding 15 % (Fig. 7). These new findings are mainly attributed to simulation times spanning a decade and boundary layer source domain. Our simulation period is significantly longer than that in previous studies where simulations over 1 year or shorter were presented. The source domains in previous studies were near the tropopause. In these studies, AM origin air was primarily transported toward the NH, with limited penetration into the higher altitudes above 450 K in the southern polar region. Our findings, in contrast, reveal a more complex pattern: AM air tends to be transported to altitudes below 450 K with transit times of less than 2 years, whereas for longer transit times, AM origin air reaches the high altitude above 450 K in the polar stratosphere via the upper branch of the BDC.

Another source of differences between the previous studies and the findings discussed here originates from the differences in the vertical position of the domain emitting the AM origin tracer. In this work, we set the source domain in the boundary layer of the AM region, while Yan et al. (2019) conducted simulations of transport from 350–360 and 370–380 K over the AM region to the global stratosphere using ERA-Interim and MERRA-2 reanalysis meteorology. Notably, Garny and Randel (2016) simulated trajectories from 360 K, but their simulation duration of just 60 d was insufficient to facilitate significant transport of AM origin air into the southern polar stratosphere. The domain considered in Yu et al. (2017) was situated immediately below the tropopause, leading to high transport contributions to the NH compared to those to the SH. Collectively, these prior studies suggest that when air is close to the tropopause, AM origin air tends to be retained more in the NH, potentially underestimating its impact on the SH, particularly in the southern polar region.

Another open question pertains to the factors contributing to the inter-annual variability in transport from source regions to the polar stratosphere. One possible influence could be the quasi-biennial oscillation (QBO). The easterly phase of the QBO in 2010 and 2013 (e.g. Anstey et al., 2022) corresponded with positive anomalies of source air in 2010 and 2013 in the northern polar stratosphere (Fig. 5j–l) and in 2011 and 2014 in the southern polar stratosphere (Fig. 5g–i). The easterly phase of the QBO induces positive upwelling anomalies near the Equator, as previously demonstrated by Baldwin et al. (2001) and Brown et al. (2023), and also influences the strength of the stratospheric polar vortex. In general, the polar vortex tends to be weaker during the easterly QBO phase when compared to the westerly phase (e.g. Holton and Tan, 1980; Pascoe et al., 2005; Watson and Gray, 2014). Therefore, the combination of stronger tropical upwelling and a weaker polar vortex transport barrier during QBO easterly phases could cause positive anomalies in SF_6 at polar latitudes. Another potential contributing mechanism could involve variations in tropical sea surface temperatures and the strength of the Asian monsoon anticyclone. Comprehensive, long-term simulations and further research efforts will be essential for gaining a deeper understanding of the mechanisms responsible for driving the inter-annual variability in transport into the polar stratosphere.

6 Conclusions

In this paper, we first quantify the air mass transport contributions from the AM region into the polar stratosphere. This quantification is achieved using artificial tracers initialized at the boundary layer within CLaMS simulations driven by ERA5 reanalysis data. Additionally, we incorporate transport from the subTR-SH to explore hemispheric differences, while transport from the tropics serves as a reference point. Notably, despite the size of the AM region being approximately 4 times smaller than that of subTR-SH, our results reveal that air mass contributions from the AM to the global stratosphere, including the southern hemispheric stratosphere, are approximately 1.5 times larger than the corresponding contributions from the subTR-SH. However, it is worth noting that transport from the tropical boundary layer still predominates. Specifically, the contributions of transport from the tropical boundary layer to the global stratosphere are roughly double those originating from the AM boundary layer. Additionally, strong downwelling and jet streams in the polar stratosphere play a vital role in isolating older stratospheric air masses within the polar vortex during local autumn and winter. Consequently, this phenomenon leads to an increase in AM tracers in the polar stratosphere below and around the vortex during these seasons. On the other hand, weak jet streams during local summer allow the isentropic transport of tropical tracers into the polar lower stratosphere.

The age spectrum analysis highlights that transport from the AM boundary layer to the polar vortex above 450 K primarily occurs at timescales exceeding 2 years, whereas transport timescales to the polar regions below the vortex are typically shorter, falling below the 2-year threshold. Our examination segregates transport contributions into two categories: those occurring within 2 years and the total contributions over the long term. This distinction reveals a notable presence of inter-annual variability in the tracer transport originating from the source domain to the polar regions. This inter-annual variability in air mass composition in the polar

vortex has the potential to propagate downward and affects also the region below the vortex. An additional factor contributing to this inter-annual variability is the influence of the shallow branch of the BDC.

Furthermore, we employ the reconstruction of SF_6 to provide further insights into the extent of transport contributions originating from the AM region. To validate the accuracy of our reconstructed SF_6 data, we compare it with SF_6 observations obtained from the ACE-FTS satellite instrument. The results demonstrate that the AM region plays a substantial role, contributing over 20 % of the SF_6 content in the polar stratosphere at altitudes above 450 K. This contribution even surpasses that of the subTR-SH despite the comparatively smaller geographical expanse of the AM domain. Importantly, more than 70 % of the subTR-NH SF_6 found in the polar regions can be attributed to transport originating in the AM region. While tropical origin air exerts the most significant influence on the composition of the polar stratosphere, our findings highlight the superior efficiency of transport from the AM boundary layer to the polar region and potentially significant influence of ozone-depleting substances from Southeast Asia on polar stratospheric chemistry, especially when accounting for the different sizes of the respective source domains.

Data availability. The SF_6 surface data are available at https://doi.org/10.15138/TQ02-ZX42 (Dutton et al., 2024). The ACE-FTS Level 2 data can be obtained via the ACE database (registration required), https://databace.scisat.ca/level2/ (University of Waterloo, 2024). The ACE-FTS data quality flags used for filtering the dataset can be accessed at https://doi.org/10.5683/SP2/BC4ATC (Sheese and Walker, 2020). The CLaMS model outputs may be obtained from the authors upon request.

Author contributions. XY conducted the ERA5-driven model simulations and performed the data analysis. PK, FP, and AP played key roles in designing the analysis, offering valuable insights through discussions, and providing constructive feedback. XY wrote the paper with contributions from all co-authors.

Competing interests. At least one of the (co-)authors is a member of the editorial board of *Atmospheric Chemistry and Physics*. The peer-review process was guided by an independent editor, and the authors also have no other competing interests to declare.

Disclaimer. Publisher's note: Copernicus Publications remains neutral with regard to jurisdictional claims made in the text, published maps, institutional affiliations, or any other geographical representation in this paper. While Copernicus Publications makes every effort to include appropriate place names, the final responsibility lies with the authors.

Acknowledgements. We thank the ECMWF for providing ERA-Interim meteorological reanalysis data for this study. We gratefully acknowledge the computing time for the CLaMS simulations granted through VSR project ID CLaMS-ESM on the supercomputer JURECA at Forschungszentrum Jülich. The authors would also like to thank the anonymous reviewers and the editor for their very insightful comments. This research has been supported by the National Natural Science Foundation of China project (grant nos. 41905040 and 42330603), the Key Laboratory of Middle Atmosphere and Global Environment Observation (grant no. LAGEO-2021-01), the Basic Research Fund of CAMS (2024Z009), and the Youth Innovation Team of China Meteorological Administration "Climate change and its impact in the Tibetan Plateauz" (CMA2023QN16). Felix Ploeger has been supported by the Deutsche Forschungsgemeinschaft (DFG, German Research Foundation; TRR 301, project ID 428312742).

Financial support. This research has been supported by the National Key Research and Development Program of China (grant no. 2023YFC3007501) and the National Natural Science Foundation of China (grant no. 42275093).

The article processing charges for this open-access publication were covered by the Forschungszentrum Jülich.

Review statement. This paper was edited by Luis Millan and reviewed by two anonymous referees.

References

Adcock, K. E., Fraser, P. J., Hall, B. D., Langenfelds, R. L., Lee, G., Montzka, S. A., Oram, D. E., Röckmann, T., Stroh, F., Sturges, W. T., Vogel, B., and Laube, J. C.: Aircraft-Based Observations of Ozone-Depleting Substances in the Upper Troposphere and Lower Stratosphere in and Above the Asian Summer Monsoon, J. Geophys. Res.-Atmos., 126, e2020JD033137, https://doi.org/10.1029/2020JD033137, 2021.

Anenberg, S. C., Miller, J., Henze, D. K., Minjares, R., and Achakulwisut, P.: The global burden of transportation tailpipe emissions on air pollution-related mortality in 2010 and 2015, Environ. Res. Lett., 14, 094012, https://doi.org/10.1088/1748-9326/ab35fc, 2019.

Anstey, J. A., Osprey, S. M., Alexander, J., Baldwin, M. P., Butchart, N., Gray, L., Kawatani, Y., Newman, P. A., and Richter, J. H.: Impacts, processes and projections of the quasi-biennial oscillation, Nature Reviews Earth & Environment, 3, 588–603, https://doi.org/10.1038/s43017-022-00323-7, 2022.

Bais, A. F., Lucas, R. M., Bornman, J. F., Williamson, C. E., Sulzberger, B., Austin, A. T., Wilson, S. R., Andrady, A. L., Bernhard, G., McKenzie, R. L., Aucamp, P. J., Madronich, S., Neale, R. E., Yazar, S., Young, A. R., de Gruijl, F. R., Norval, M., Takizawa, Y., Barnes, P. W., Robson, T. M., Robinson, S. A., Ballaré, C. L., Flint, S. D., Neale, P. J., Hylander, S., Rose, K. C., Wängberg, S.-Å., Häder, D.-P., Worrest, R. C., Zepp, R. G., Paul, N. D., Cory, R. M., Solomon, K. R., Longstreth, J., Pandey, K. K., Redhwi, H. H., Torikai, A., and Heikkilä, A. M.: Envi-

ronmental effects of ozone depletion, UV radiation and interactions with climate change: UNEP Environmental Effects Assessment Panel, update 2017, Photochem. Photobio. S., 17, 127–179, https://doi.org/10.1039/C7PP90043K, 2018.

Baldwin, M., Gray, L., Dunkerton, T., Hamilton, K., Haynes, P., Randel, W., Holton, J., Alexander, M., Hirota, I., Horinouchi, T., Jones, D., Kinnersley, J., Marquardt, C., Sato, K., and Takahashi, M.: The quasi-biennial oscillation, Rev. Geophys., 39, 179–229, 2001.

Bergman, J. W., Jensen, E. J., Pfister, L., and Yang, Q.: Seasonal differences of vertical-transport efficiency in the tropical tropopause layer: On the interplay between tropical deep convection, large-scale vertical ascent, and horizontal circulations, J. Geophys. Res., 117, D05302, https://doi.org/10.1029/2011JD016992, 2012.

Bernath, P. F., McElroy, C. T., Abrams, M. C., Boone, C. D., Butler, M., Camy-Peyret, C., Carleer, M., Clerbaux, C., Coheur, P.-F., Colin, R., DeCola, P., DeMazière, M., Drummond, J. R., Dufour, D., Evans, W. F. J., Fast, H., Fussen, D., Gilbert, K., Jennings, D. E., Llewellyn, E. J., Lowe, R. P., Mahieu, E., McConnell, J. C., McHugh, M., McLeod, S. D., Michaud, R., Midwinter, C., Nassar, R., Nichitiu, F., Nowlan, C., Rinsland, C. P., Rochon, Y. J., Rowlands, N., Semeniuk, K., Simon, P., Skelton, R., Sloan, J. J., Soucy, M.-A., Strong, K., Tremblay, P., Turnbull, D., Walker, K. A., Walkty, I., Wardle, D. A., Wehrle, V., Zander, R., and Zou, J.: Atmospheric Chemistry Experiment (ACE) Mission overview, Geophys. Res. Lett., 32, L15S01, https://doi.org/10.1029/2005GL022386, 2005.

Berntsen, T. K., Karlsdóttir, S. N., and Jaffe, D. A.: Influence of Asian emissions on the composition of air reaching the north western United States, Geophys. Res. Lett., 26, 2171–2174, 1999.

Bian, J., Li, D., Bai, Z., Li, Q., Lyu, D., and Zhou, X.: Transport of Asian surface pollutants to the global stratosphere from the Tibetan Plateau region during the Asian summer monsoon, Natl. Sci. Rev., 7, 516–533, https://doi.org/10.1093/nsr/nwaa005, 2020.

Brown, F., Marshall, L., Haynes, P. H., Garcia, R. R., Birner, T., and Schmidt, A.: On the magnitude and sensitivity of the quasi-biennial oscillation response to a tropical volcanic eruption, Atmos. Chem. Phys., 23, 5335–5353, https://doi.org/10.5194/acp-23-5335-2023, 2023.

Chirkov, M., Stiller, G. P., Laeng, A., Kellmann, S., von Clarmann, T., Boone, C. D., Elkins, J. W., Engel, A., Glatthor, N., Grabowski, U., Harth, C. M., Kiefer, M., Kolonjari, F., Krummel, P. B., Linden, A., Lunder, C. R., Miller, B. R., Montzka, S. A., Mühle, J., O'Doherty, S., Orphal, J., Prinn, R. G., Toon, G., Vollmer, M. K., Walker, K. A., Weiss, R. F., Wiegele, A., and Young, D.: Global HCFC-22 measurements with MIPAS: retrieval, validation, global distribution and its evolution over 2005–2012, Atmos. Chem. Phys., 16, 3345–3368, https://doi.org/10.5194/acp-16-3345-2016, 2016.

Clem, K. R., Fogt, R. L., Turner, J., Lintner, B. R., Marshall, G. J., Miller, J. R., and Renwick, J. A.: Record warming at the South Pole during the past three decades, Nat. Clim. Change, 10, 762–770, https://doi.org/10.1038/s41558-020-0815-z, 2020.

Denning, A. S., Holzer, M., Gurney, K. R., Heimann, M., Law, R. M., Rayner, P. J., Fung, I. Y., Fan, S.-M., Taguchi, S., Friedlingstein, P., Balkanski, Y., Taylor, J., Maiss, M., and Levin, I.: Three-dimensional transport and concentration of SF_6 A model intercomparison study (TransCom 2), Tellus B, 51, 266–297, https://doi.org/10.3402/tellusb.v51i2.16286, 1999.

Dethof, A., O'Neill, A., Slingo, J. M., and Smit, H. G. J.: A mechanism for moistening the lower stratosphere involving the Asian summer monsoon, Q. J. Roy. Meteor. Soc., 556, 1079–1106, 1999.

Dutton, G. S., Hall, B. D., Dlugokencky, E. J., Lan, X., Madronich, M., Nance, J. D., and Petersen, K. M.: Combined Atmospheric Sulfur hexaflouride Dry Air Mole Fractions from the NOAA GML Halocarbons Sampling Network, 1995–2024, Version: 2024-02-21, Global Monitoring Laboratory [data set], https://doi.org/10.15138/TQ02-ZX42, 2024.

Fadnavis, S., Roy, C., Chattopadhyay, R., Sioris, C. E., Rap, A., Müller, R., Kumar, K. R., and Krishnan, R.: Transport of trace gases via eddy shedding from the Asian summer monsoon anticyclone and associated impacts on ozone heating rates, Atmos. Chem. Phys., 18, 11493–11506, https://doi.org/10.5194/acp-18-11493-2018, 2018.

Garny, H. and Randel, W. J.: Transport pathways from the Asian monsoon anticyclone to the stratosphere, Atmos. Chem. Phys., 16, 2703–2718, https://doi.org/10.5194/acp-16-2703-2016, 2016.

Granier, C., Bessagnet, B., Bond, T. C., D'Angiola, A., Denier van der Gon, H., Frost, G. J., Heil, A., Kaiser, J. W., Kinne, S., Klimont, Z., Kloster, J., Lamarque, J. F., Liousse, C., Masui, T., Meleux, F., Mieville, A., Ohara, T., Raut, J.-C., Riahi, K., Schultz, M., Smith, S. J., Thomson, A. M., van Aardenne, J., van der Werf, G. R., and Van Vuuren, D.: Evolution of anthropogenic and biomass burning emissions of air pollutants at global and regional scales during the 1980–2010 period, Climatic Change, 109, 163–190, https://doi.org/10.1007/s10584-011-0154-1, 2011.

Haine, T. W. N., Zhang, H., Waugh, D. W., and Holzer, M.: On transit time distributions in unsteady circulation models, Ocean Model., 21, 35–45, 2008.

Holton, J. R. and Tan, H.-C.: The influence of the equatorial quasi-biennial oscillation on the global circulation at 50 mb, J. Atmos. Sci., 37, 2200–2208, 1980.

Janssens-Maenhout, G., Crippa, M., Guizzardi, D., Muntean, M., Schaaf, E., Dentener, F., Bergamaschi, P., Pagliari, V., Olivier, J. G. J., Peters, J. A. H. W., van Aardenne, J. A., Monni, S., Doering, U., Petrescu, A. M. R., Solazzo, E., and Oreggioni, G. D.: EDGAR v4.3.2 Global Atlas of the three major greenhouse gas emissions for the period 1970–2012, Earth Syst. Sci. Data, 11, 959–1002, https://doi.org/10.5194/essd-11-959-2019, 2019.

Konopka, P., Steinhorst, H.-M., Grooß, J.-U., Günther, G., Müller, R., Elkins, J. W., Jost, H.-J., Richard, E., Schmidt, U., Toon, G., and McKenna, D. S.: Mixing and Ozone Loss in the 1999–2000 Arctic Vortex: Simulations with the 3-dimensional Chemical Lagrangian Model of the Stratosphere (CLaMS), J. Geophys. Res., 109, D02315, https://doi.org/10.1029/2003JD003792, 2004.

Konopka, P., Tao, M., von Hobe, M., Hoffmann, L., Kloss, C., Ravegnani, F., Volk, C. M., Lauther, V., Zahn, A., Hoor, P., and Ploeger, F.: Tropospheric transport and unresolved convection: numerical experiments with CLaMS 2.0/MESSy, Geosci. Model Dev., 15, 7471–7487, https://doi.org/10.5194/gmd-15-7471-2022, 2022.

Kurokawa, J., Ohara, T., Morikawa, T., Hanayama, S., Janssens-Maenhout, G., Fukui, T., Kawashima, K., and Akimoto, H.: Emissions of air pollutants and greenhouse gases over Asian regions during 2000–2008: Regional Emission inventory in ASia (REAS) version 2, Atmos. Chem. Phys., 13, 11019–11058, https://doi.org/10.5194/acp-13-11019-2013, 2013.

Li, F., Waugh, D. W., Douglass, A. R., Newman, P. A., Pawson, S., Stolarski, R. S., Strahan, S. E., and Nielsen, J. E.: Seasonal variations in stratospheric age spectra in GEOSCCM, J. Geophys. Res., 117, D05134, https://doi.org/10.1029/2011JD016877, 2012.

Ma, D., Wang, T., Wu, H., Qu, Y., Li, S., Zhuang, B., Li, M., Xie, M., and Kilifarska-Nedialkova, N. A.: The joint impact of $PM_{2.5}$, O_3, and CO_2 on the East Asian Summer Monsoon in 2013 and 2018 due to contrasting emission reduction, Atmos. Environ., 333, 120678, https://doi.org/10.1016/j.atmosenv.2024.120678, 2024.

McKenna, D. S., Konopka, P., Grooß, J.-U., Günther, G., Müller, R., Spang, R., Offermann, D., and Orsolini, Y.: A new Chemical Lagrangian Model of the Stratosphere (CLaMS): 1. Formulation of advection and mixing, J. Geophys. Res., 107, 4309, https://doi.org/10.1029/2000JD000114, 2002.

Montzka, S. A., Dutton, G. S., Yu, P., Ray, E. A., Portmann, R. W., Daniel, J., Kuijpers, L. J. M., Hall, B. D., Mondeel, D. J., Siso, C., Nance, J. D., Rigby, M. L., Manning, A. J., Hu, L., Moore, F. L., Miller, B. R., and Elkins, J. W.: An unexpected and persistent increase in global emissions of ozone-depleting CFC-11, Nature, 557, 413–417, 2018.

Nützel, M., Podglajen, A., Garny, H., and Ploeger, F.: Quantification of water vapour transport from the Asian monsoon to the stratosphere, Atmos. Chem. Phys., 19, 8947–8966, https://doi.org/10.5194/acp-19-8947-2019, 2019.

Orbe, C., Waugh, D. W., and Newman, P. A.: Air-mass origin in the tropical lower stratosphere: The influence of Asian boundary layer air, Geophys. Res. Lett., 42, 4240–4248, https://doi.org/10.1002/2015GL063937, 2015.

Pan, L. L., Honomichl, S. B., Kinnison, D. E., Abalos, M., Randel, W. J., Bergman, J. W., and Bian, J.: Transport of chemical tracers from the boundary layer to stratosphere associated with the dynamics of the Asian summer monsoon, J. Geophys. Res.-Atmos., 121, 14159–14174, https://doi.org/10.1002/2016JD025616, 2016.

Park, M., Randel, W. J., Emmons, L. K., and Livesey, N. J.: Transport pathways of carbon monoxide in the Asian summer monsoon diagnosed from Model of Ozone and Related Tracers (MOZART), J. Geophys. Res., 114, D08303, https://doi.org/10.1029/2008JD010621, 2009.

Park, M., Randel, W. J., Kinnison, D. E., Emmons, L. K., Bernath, P. F., Walker, K. A., Boone, C. D., and Livesey, N. J.: Hydrocarbons in the upper troposphere and lower stratosphere observed from ACE-FTS and comparisons with WACCM, J. Geophys. Res.-Atmos., 118, 1964–1980, https://doi.org/10.1029/2012JD018327, 2013.

Pascoe, C. L., Gray, L. J., Crooks, S. A., Juckes, M. N., and Baldwin, M. P.: The quasi-biennial oscillation: Analysis using ERA-40 data, J. Geophys. Res.-Atmos., 110, D08105, https://doi.org/10.1029/2004JD004941, 2005.

Ploeger, F. and Birner, T.: Seasonal and inter-annual variability of lower stratospheric age of air spectra, Atmos. Chem. Phys., 16, 10195–10213, https://doi.org/10.5194/acp-16-10195-2016, 2016.

Ploeger, F., Konopka, P., Walker, K., and Riese, M.: Quantifying pollution transport from the Asian monsoon anticyclone into the lower stratosphere, Atmos. Chem. Phys., 17, 7055–7066, https://doi.org/10.5194/acp-17-7055-2017, 2017.

Ploeger, F., Legras, B., Charlesworth, E., Yan, X., Diallo, M., Konopka, P., Birner, T., Tao, M., Engel, A., and Riese, M.: How robust are stratospheric age of air trends from different reanalyses?, Atmos. Chem. Phys., 19, 6085–6105, https://doi.org/10.5194/acp-19-6085-2019, 2019.

Podglajen, A. and Ploeger, F.: Retrieving the age of air spectrum from tracers: principle and method, Atmos. Chem. Phys., 19, 1767–1783, https://doi.org/10.5194/acp-19-1767-2019, 2019.

Pommrich, R., Müller, R., Grooß, J.-U., Konopka, P., Ploeger, F., Vogel, B., Tao, M., Hoppe, C. M., Günther, G., Spelten, N., Hoffmann, L., Pumphrey, H.-C., Viciani, S., D'Amato, F., Volk, C. M., Hoor, P., Schlager, H., and Riese, M.: Tropical troposphere to stratosphere transport of carbon monoxide and long-lived trace species in the Chemical Lagrangian Model of the Stratosphere (CLaMS), Geosci. Model Dev., 7, 2895–2916, https://doi.org/10.5194/gmd-7-2895-2014, 2014.

Randel, W. J., Park, M., Emmons, L., Kinnison, D., Bernath, P., Walker, K. A., Boone, C., and Pumphrey, H.: Asian Monsoon Transport of Pollution to the Stratosphere, Science, 328, 611–613, https://doi.org/10.1126/science.1182274, 2010.

Riese, M., Ploeger, F., Rap, A., Vogel, B., Konopka, P., Dameris, M., and Forster, P.: Impact of uncertainties in atmospheric mixing on simulated UTLS composition and related radiative effects, J. Geophys. Res., 117, D16305, https://doi.org/10.1029/2012JD017751, 2012.

Rolf, C., Vogel, B., Hoor, P., Afchine, A., Günther, G., Krämer, M., Müller, R., Müller, S., Spelten, N., and Riese, M.: Water vapor increase in the lower stratosphere of the Northern Hemisphere due to the Asian monsoon anticyclone observed during the TACTS/ESMVal campaigns, Atmos. Chem. Phys., 18, 2973–2983, https://doi.org/10.5194/acp-18-2973-2018, 2018.

Santee, M. L., Manney, G. L., Livesey, N. J., Schwartz, M. J., Neu, J. L., and Read, W. G.: A comprehensive overview of the climatological composition of the Asian summer monsoon anticyclone based on 10 years of Aura Microwave Limb Sounder measurements, J. Geophys. Res.-Atmos., 122, 5491–5514, https://doi.org/10.1002/2016JD026408, 2017.

Sheese, P. and Walker, K.: Data Quality Flags for ACE-FTS Level 2 Version 4.1/4.2 Data Set, Version V41, Borealis [data set], https://doi.org/10.5683/SP2/BC4ATC, 2020.

Tessum, M. W., Anenberg, S. C., Chafe, Z. A., Henze, D. K., Kleiman, G., Kheirbek, I., Marshall, J. D., and Tessum, C. W.: Sources of ambient $PM_{2.5}$ exposure in 96 global cities, Atmos. Environ., 286, 119234, https://doi.org/10.1016/j.atmosenv.2022.119234, 2022.

Tritscher, I., Pitts, M. C., Poole, L. R., Alexander, S. P., Cairo, F., Chipperfield, M. P., Grooß, J.-U., Höpfner, M., Lambert, A., Luo, B., Molleker, S., Orr, A., Salawitch, R., Snels, M., Spang, R., Woiwode, W., and Peter, T.: Polar Stratospheric Clouds: Satellite Observations, Processes, and Role in Ozone Depletion, Rev. Geophys., 59, e2020RG000702, https://doi.org/10.1029/2020RG000702, 2021.

Tzella, A. and Legras, B.: A Lagrangian view of convective sources for transport of air across the Tropical Tropopause Layer: distribution, times and the radiative influence of clouds, Atmos. Chem. Phys., 11, 12517–12534, https://doi.org/10.5194/acp-11-12517-2011, 2011.

University of Waterloo: ACE-FTS Level 2 data, ACE database, https://databace.scisat.ca/level2/ (last access: 27 January 2025), 2024.

Vernier, J.-P., Thomason, L. W., and Kar, J.: CALIPSO detection of an Asian tropopause aerosol layer, Geophys. Res. Lett., 38, L07804, https://doi.org/10.1029/2010GL046614, 2011.

Vogel, B., Günther, G., Müller, R., Grooß, J.-U., and Riese, M.: Impact of different Asian source regions on the composition of the Asian monsoon anticyclone and of the extratropical lowermost stratosphere, Atmos. Chem. Phys., 15, 13699–13716, https://doi.org/10.5194/acp-15-13699-2015, 2015.

Vogel, B., Günther, G., Müller, R., Grooß, J.-U., Afchine, A., Bozem, H., Hoor, P., Krämer, M., Müller, S., Riese, M., Rolf, C., Spelten, N., Stiller, G. P., Ungermann, J., and Zahn, A.: Long-range transport pathways of tropospheric source gases originating in Asia into the northern lower stratosphere during the Asian monsoon season 2012, Atmos. Chem. Phys., 16, 15301–15325, https://doi.org/10.5194/acp-16-15301-2016, 2016.

Wang, H., Lu, X., Jacob, D. J., Cooper, O. R., Chang, K.-L., Li, K., Gao, M., Liu, Y., Sheng, B., Wu, K., Wu, T., Zhang, J., Sauvage, B., Nédélec, P., Blot, R., and Fan, S.: Global tropospheric ozone trends, attributions, and radiative impacts in 1995–2017: an integrated analysis using aircraft (IAGOS) observations, ozonesonde, and multi-decadal chemical model simulations, Atmos. Chem. Phys., 22, 13753–13782, https://doi.org/10.5194/acp-22-13753-2022, 2022.

Wang, Y., Yuan, Q., Li, T., and Zhu, L.: Global spatiotemporal estimation of daily high-resolution surface carbon monoxide concentrations using Deep Forest, J. Clean. Prod., 350, 131500, https://doi.org/10.1016/j.jclepro.2022.131500, 2022.

Watson, P. A. G. and Gray, L. J.: How Does the Quasi-Biennial Oscillation Affect the Stratospheric Polar Vortex?, J. Atmos. Sci., 71, 391–409, https://doi.org/10.1175/JAS-D-13-096.1, 2014.

Waugh, D. W., Crotwell, A. M., Dlugokencky, E. J., Dutton, G. S., Elkins, J. W., Hall, B. D., Hintsa, E. J., Hurst, D. F., Montzka, S. A., Mondeel, D. J., Moore, F. L., Nance, J. D., Ray, E. A., Steenrod, S. D., Strahan, S. E., and Sweeney, C.: Tropospheric SF6: Age of air from the Northern Hemisphere midlatitude surface, J. Geophys. Res., 118, 11429–11441, 013.

World Meteorological Organization: Scientific assessment of ozone depletion: 2022, GAW Report No. 278, Geneva, Switzerland, ISBN 978-9914-733-97-6, https://ozone.unep.org/science/assessment/sap (last access: 24 January 2025), 2022.

Wright, J. S., Fu, R., Fueglistaler, S., Liu, Y. S., and Zhang, Y.: The influence of summertime convection over Southeast Asia on water vapor in the tropical stratosphere, J. Geophys. Res., 116, D12302, https://doi.org/10.1029/2010JD015416, 2011.

Yan, X., Konopka, P., Ploeger, F., Podglajen, A., Wright, J. S., Müller, R., and Riese, M.: The efficiency of transport into the stratosphere via the Asian and North American summer monsoon circulations, Atmos. Chem. Phys., 19, 15629–15649, https://doi.org/10.5194/acp-19-15629-2019, 2019.

Yan, X., Konopka, P., Hauck, M., Podglajen, A., and Ploeger, F.: Asymmetry and pathways of inter-hemispheric transport in the upper troposphere and lower stratosphere, Atmos. Chem. Phys., 21, 6627–6645, https://doi.org/10.5194/acp-21-6627-2021, 2021.

Yu, P., Rosenlof, K. H., Liu, S., Telg, H., Thornberry, T. D., Rollins, A. W., Portmann, R. W., Bai, Z., Ray, E. A., Duan, Y., Pan, L. L., Toon, O. B., Bian, J., and Gao, R.-S.: Efficient transport of tropospheric aerosol into the stratosphere via the Asian summer monsoon anticyclone, P. Natl. Acad. Sci. USA, 114, 6972–6977, https://doi.org/10.1073/pnas.1701170114, 2017.